J Mater Sci (2019) 54:2059–2065

Chemical routes to materials

Hydrothermal synthesis and fast photoresponsive characterization of SnS_2 hexagonal nanoflakes

He Tian[1], Chao Fan[1,*], Gangzha Liu[1], Yonghui Zhang[1], Mengjun Wang[1], and Erping Li[1,*]

[1] *Institute of Micro-Nano Photoelectron and Electromagnetic Technology Innovation, School of Electronics and Information Engineering, Hebei University of Technology, Tianjin 300401, People's Republic of China*

Received: 7 August 2018
Accepted: 20 September 2018
Published online: 25 September 2018

ABSTRACT

As an emerging material of layered metal dichalcogenides (LMDs), tin disulfide (SnS_2) has huge potentials in visible-light detectors and photovoltaic devices due to its 2.0–2.6 eV band gap. However, its photoresponsive characteristic is still relative rarely investigated compared to other LMDs, such as MoS_2. Herein, SnS_2 nanoflakes are synthesized by a facile and fruitful hydrothermal method, and photoresponsive characteristics are investigated. At first detailed phase structure, morphology and constitution are characterized. This SnS_2 is flake-like with a mean diameter of ~ 500 nm, and the atomic ratio of Sn to S is 1:2.1. Furthermore, prototype photodetectors are fabricated and characterized to explore photoresponsive characteristics of these SnS_2 nanoflakes. The results show that SnS_2 nanoflakes have excellently stable and repeatable photoresponse property to 532 nm and 405 nm incidents. In particular, it reveals a fast response time of 7.3 ms to the 405 nm incident, which enables SnS_2 nanoflakes promising candidate for photodetectors.

Introduction

Two-dimensional layered metal dichalcogenides (LMDs) materials including molybdenum disulfide (MoS_2), tungsten disulfide (WS_2) and black phosphorus have attracted a huge of interests in the last decade due to their graphene-like structures, various energy band gaps, excellent mechanical properties, high transparency and unique optoelectronic properties [1]. By taking advantage of these features, new type of electronic and optoelectronic devices has appeared and been developed, including tunnel transistor, flexible electronics, photovoltaics and light-emitting devices. As an emerging material of LMDs, tin disulfide (SnS_2) is an n-type indirect bandgap semiconductor with a band gap ranging from 2.0 to 2.6 eV [2, 3]. It has a layered sandwich structure, and every two adjacent layers of S–Sn–S interacted with each other by Van der Waals forces. In addition, its component elements Sn and S are earth abundant and environment friendly [4]. Sn element has good chemical activity, and nanomaterials based on Sn have various applications [5–8]. And the electronic, physical and chemical properties

Address correspondence to E-mail: fanch@hebut.edu.cn; liep@zju.edu.cn

https://doi.org/10.1007/s10853-018-2959-z

of SnS_2 have been extensively studied, and SnS_2 has promising uses in solar cell [9], lithium battery [10], flexible devices [11] and optoelectronic devices [12]. Moreover, photodetectors and photovoltaic devices are important potential applications of SnS_2. Nevertheless, researches on the photosensitive properties of SnS_2 nanoflakes are less performed.

In this work, we synthesized SnS_2 nanoflakes (NFs) via a hydrothermal method using stannic chloride pentahydrate ($SnCl_4{\cdot}5H_2O$) and thiourea (CH_4N_2S) as precursors [13]. Furthermore, we fabricated simple prototype photodetectors based on the as-synthesized SnS_2 NFs to explore the photoresponsive characteristic of the SnS_2. Impressively, SnS_2 NFs-based photodetectors exhibited high photodetection performance with a fast response time of 7.3 ms and high detectivity of 1.53×10^{10} jones. Thus, the excellent optical response characteristics of the device, such as stability and repeatability, as well as fast response time, cater well to the requirements for the next-generation photovoltaic devices, making the SnS_2 NFs a promising component of high-performance optoelectronic devices.

Experiment section

Synthesis of SnS_2 nanoflakes

SnS_2 was synthesized in a 50-ml stainless steel autoclave by a facile hydrothermal method. Analytical grade stannic chloride pentahydrate ($SnCl_4{\cdot}5H_2O$) and thiourea (CH_4N_2S) were used as precursor reagents to make a suitable amount of stoichiometric mixture in autoclave. Thirty milliliter distilled water was added into the autoclave and stirred for 1 h. Then, the autoclave was sealed and maintained at 180 °C for 24 h, and the furnace cooled to room temperature naturally. The products were collected by centrifugation and well washed with absolute ethanol and distilled water twice before drying in a vacuum box at 50 °C for 12 h [14].

Characterization

Morphology and phase structure are characterized by a scanning electron microscopy (SEM, FEI Nano-SEM450) and an X-ray diffraction (XRD, Rigaku, Smartlab) using Cu Ka radiation (λ = 0.15406 nm). The elemental composition was investigated by an X-ray photoelectrons Spectroscopy (XPS, Thermo Escalab 250Xi) and an energy-dispersive spectroscopy (EDS, AMETEK Octane Plus). And the vibrational modes were studied by a micro-Raman spectrometer (Renishaw inVia, 532 nm laser excitation).

Device fabrication and measurement

Devices based on the as-synthesized SnS_2 NFs were fabricated to investigate their photoresponsive characteristics. Firstly, an ITO glass was separated by a non-conducting gap with a width of $\sim$ 50 μm. Secondly the SnS_2 NFs were dispersed in ethanol and then deposited on the glass. Finally, the gap was fulfilled with the SnS_2 NFs. For these obtained devices, all electrical measurements were taken using a semiconductor device analyzer (Keysight, B1500A).

Results and discussion

Figure 1a shows a panoramic SEM image of the SnS_2 NFs obtained at 180 °C for 24 h, and a 4 times zoom-in image is presented in Fig. 1b. It can be seen that the as-synthesized products have distinct hexagonal flake-like structures, with plane surfaces, a mean diameter of $\sim$ 500 nm and an average thickness of $\sim$ 40 nm. The NFs aggregate together with random directions. EDS measurements were also taken, and the result shows the atomic ratio of Sn to S is probably 1:2.1. XRD measurements were taken, and Fig. 1c depicts the obtained XRD pattern of the as-synthesized SnS_2 NFs. The XRD patterns were well indexed to the pure hexagonal phase of H-SnS_2 (JCPDS No. 23-0677) with the lattice constants a = 3.648 Å and c = 5.899 Å and the space group P-3m1, and the corresponding Miller indices were also marked. Sharp diffraction peaks demonstrate high crystallinity of the as-synthesized SnS_2. No other phases or impurities such as $SnCl_4$, S and SnS were detected [15]. Raman spectroscopy was used to study vibrational modes of the SnS_2 NFs. As illustrated in Fig. 1d, there is only one peak located at 315 cm^{-1}, and it is assigned to the A_{1g} phonon mode of SnS_2, which is consistent with a previous report [16, 17].

The chemical composition of the SnS_2 NFs was determined by XPS, and the results are illustrated in Fig. 1d. The peak at 162.1 eV corresponds to the binding energy of S^{2-} 2p, and the corresponding

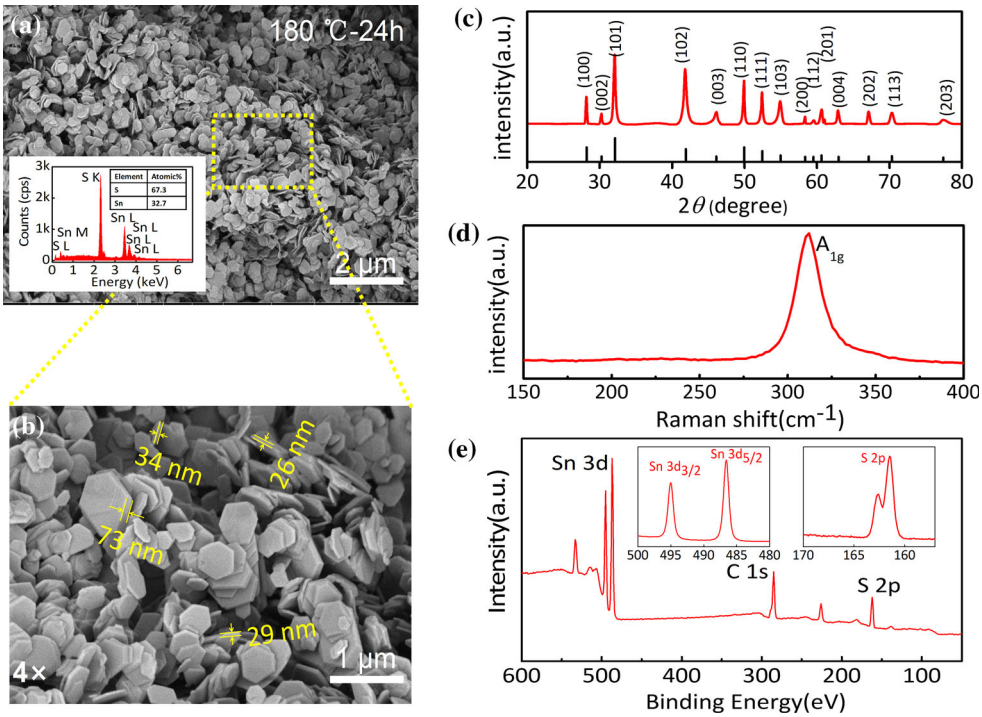

Figure 1 **a**, **b** Panoramic SEM image of the as-synthesized products grown at 180 °C for 24 h and 4 times enlarged image. The inset is the EDS spectrum of the SnS_2 NFs. **c** XRD pattern, **d** Raman spectrum and **e** XPS spectrum of the SnS_2 NFs.

binding energy of Sn^{4+} $3d_{3/2}$ and Sn^{4+} $3d_{5/2}$ is 495 and 486.6 eV, respectively. The atomic ratio of the as-synthesized SnS_2 is defined as $A_{Sn:S} = \frac{I_1/S_1}{I_2/S_2}$, where I_1 and I_2 are relative areas under the Sn and S peaks, respectively. S_1 and S_2 are the corresponding sensitivity factors, which are 3.2 and 0.35, respectively. By calculation, the ratio of the SnS_2 NFs is 1:2.1, which is consistent with the EDS analysis. According to the results above, it is confirmed that the hydrothermal synthesized SnS_2 NFs have high crystallinity and purity.

In order to explore the growth process and influence parameters during hydrothermal synthesis of the as-synthesized SnS_2, samples under different conditions were prepared. Figure 2a–c shows SEM images of the products grown at different reaction times from 8 to 16 h. And Fig. 2d-f shows SEM images of the products synthesized at different temperatures from 120 to 180 °C. As the reaction time increased, SnS_2 became bigger and more regular. Meanwhile, their differences became smaller and smaller, while morphology depicted in Fig. 2f is much different from the others. The products synthesized at 120 °C are gel-like and probably amorphous. Morphologies of the products synthesized at 140 and 160 °C are similar. The products obtained at higher reaction temperature are larger and more regular, which indicates better crystallinity.

XRD patterns of the products obtained under different conditions are also shown in Fig. 2g and h. In Fig. 2g, the intensity of these diffraction peaks increase with temperature, which indicates SnS_2 with better crystallinity can be obtained at a higher reaction temperature. Moreover, there only some smooth peak envelopes can be found in the XRD pattern of the products grown at 120 °C, indicating the products should be amorphous. XRD patterns are similar in Fig. 2h, except that the intensity of some diffraction peaks is slightly different.

The whole synthesis process can be divided into two reactions process, which can be expressed as below:

$$SC(H_2N)_2 + H_2O \rightarrow CO_2 + NH_3 + H_2S \quad (1)$$

$$SnCl_4 + NH_3 + H_2S \rightarrow NH_4Cl + SnS_2 \quad (2)$$

At the first step, thiourea was hydrolyzed, and released S^{2-} ions at high temperature. Then stannic chloride pentahydrate reacted with S^{2-} ions, and precipitates were synthesized at the second step. The whole reaction was both effected by temperature and reaction time. However, the hydrolyzation of the thiourea was more effected by temperature than reaction time. Consequently, it is concluded by

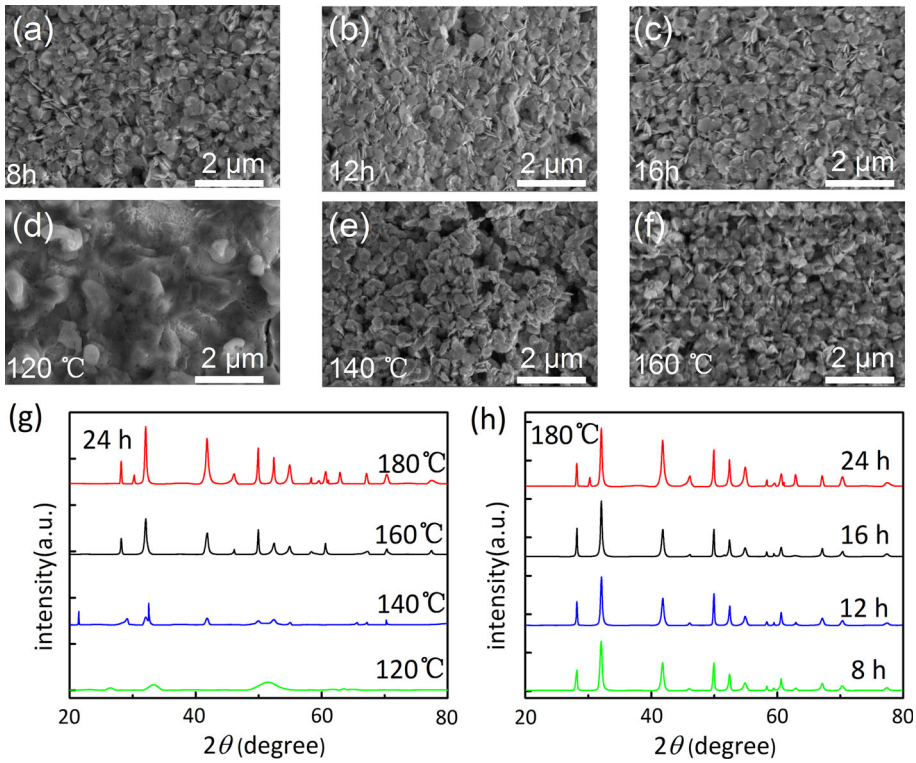

Figure 2 SEM images of the products synthesized for different reaction times (**a**–**c**) and different reaction temperatures (**d**–**f**). **g** XRD patterns of the products synthesized at different reaction temperatures ranging from 120 to 180 °C. **h** XRD patterns of the products synthesized for different reaction times ranging from 8 to 24 h.

comparison that the reaction temperature is a more important parameter than the reaction time for the synthesis of SnS_2 by hydrothermal method.

The schematic diagram of a prototype SnS_2 photodetector is illustrated in Fig. 3a. The gap between two electrodes is ~ 50 um. And the as-synthesized SnS_2 filled in the gap. Figure 3b and c shows the current (I)–voltage (V) characteristics of the as-synthesized SnS_2-based photodetector under illumination of a green laser and blue laser with different light power intensities. The wavelength of the green laser and the blue laser is 532 nm and 405 nm, separately. The I–V curves with the applied voltage ranging from − 3 to 3 V indicate good ohmic contacts. The photocurrent I_{ph} is defined as $I_{ph} = I_{illuminated} - I_{dark}$, and I_{ph} increased as light power intensities increased [18]. The relationship between light power intensity and photocurrent was studied, and I_{ph} as a function of light power intensity is shown in the inset of Fig. 3. By fitting the data, I_{ph} can be expressed by the equation of $I_{ph} = aP^{\alpha}$, where a and α are 5.67×10^{-12} and 0.68 for the green laser, 3.78×10^{-11} and 0.48 for the blue laser, respectively. The deviation of the ideal index of $\alpha = 1$ means that the light energy converted from the external light energy to the current is lost, which is related to the complicated process of photon absorption, electron hole separation, and carrier transport.

Three important parameters for characterizing the performance of the photodetector are the photoresponsivity (R), external quantum efficiency (EQE) and detectivity (D^*) [19]. The R can be defined as $R = I_{ph}/PS$, where I_{ph} is the photocurrent, P is the light power intensity, and S is the effective exposure area of the photodetector. For the device under illumination of the green laser, R is calculated to be 4.64 mA W^{-1}. The EQE can be expressed by the equation of $EQE = hcR/e\lambda$, where h is Planck's constant, c is the light velocity, e is the electron charge, and λ is the incident light wavelength. Based on these data, the EQE is about 1.08% for the green laser. In addition, photosensitivity reveals the sensitivity of photodetector, which can be defined as $D^* = \frac{RS^{1/2}}{(2eI_{dark})^{1/2}}$, where I_{dark} is the dark current. The calculated D^* for the green laser is 1.2×10^9 jones. Similarly for the blue laser, the R calculated is about 58.5 mA W^{-1}, the EQE is about 17.9%, and the D^* is about 1.53×10^{10} jones, which is comparable to $MoSe_2$, graphene and other materials [20]. The relatively low R and EQE compared with other SnS_2 monolayer and multilayers are probably due to two reasons [21]. One is the as-synthesized SnS_2 was aggregated NFs, whose scale

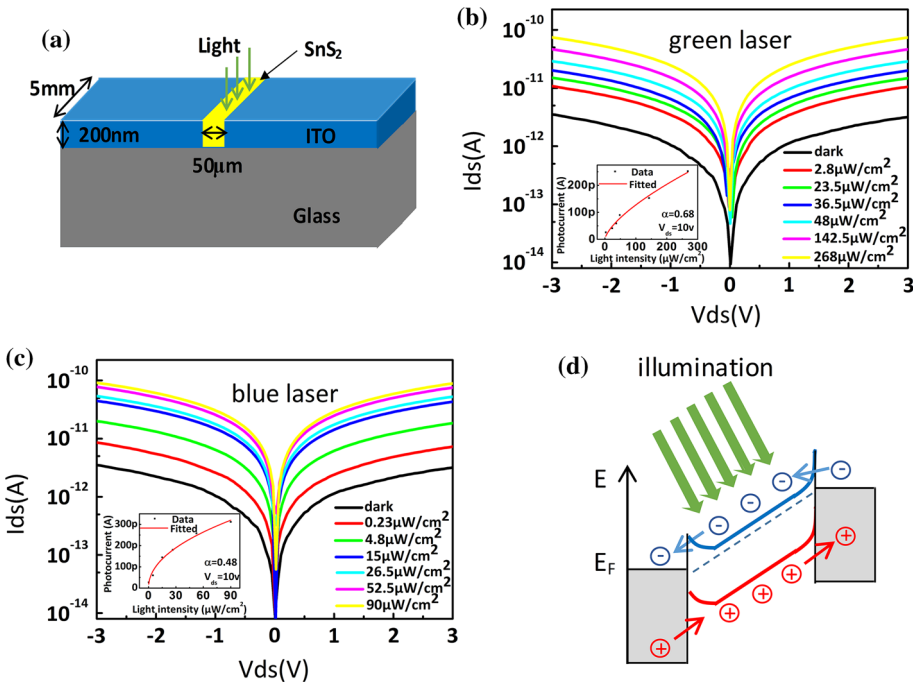

Figure 3 **a** Schematic illustration of the single SnS_2 NFs-based photodetector device configuration for photocurrent measurements. **b**, **c** *I–V* characteristics in logarithmic coordinates of the device in the dark and in the presence of the green laser (**b**, 532 nm) and blue laser (**c**, 405 nm) illumination with different light power intensities. Inset in **b**, **c** shows the light power intensity dependence of the photocurrent under the bias voltage of 10 V. **d** Energy band diagrams of a SnS_2 NFs-based device.

and thickness limited the performance of the photodetector. The other is the prototype photodetector was simple, and the existence of crystal boundaries hampered the transport of free electrons.

The photoresponsive processes of SnS_2-based photodetectors were further studied. And the corresponding mechanism is proposed in Fig. 3d. Under the bias voltage and without illumination, there is a small current, which is called as the "OFF" state. While the laser is switched on and shined on the devices, the absorbed photons transit electrons located in valence band directly to conduction band. And the free carriers increase due to photon absorption, leading to the reduction in the semiconductor resistance. The newly photogenerated free electrons and holes shift in opposite directions under bias voltage and result in photocurrent [22, 23]. The state is called the "ON" state. When the laser is switched off, excited electrons in conduction band decrease rapidly and return to valence through radiative recombination transition. And the devices recover to original "OFF" state. With the intermittent illumination of lasers, the photodetector transforms between "ON" and "OFF" states and forms a stable and periodic process.

The time-resolved photoresponse of the device was also measured under illumination of lasers with different wavelengths (green, 532 nm; blue, 405 nm) and different light power intensities (0.317, 0.41 and 0.54 mW/cm^2 for the green laser; 0.031, 0.058 and 0.098 mW/cm^2 for the blue laser), and the results are depicted in Fig. 4a and b. The external bias voltage was set as 5 V. The curves of the device exhibit good stability and repeatability. The response and decay time are also critical parameters of evaluating the performance of the photodetector. Figure 4c–f shows the response and decay curves under illuminations of the green and blue lasers. In addition, in order to calculate the response time (τ_r) and decay time (τ_f) more accurately, we have fitted the curve in Fig. 4c–f, and the two fitting formulas are followed [24]:

$$I_{ds} = I - I_0 \times \exp[-(t - t_0)/\tau_r] \quad (3)$$

$$I_{ds} = I + I_0 \times \exp[-(t - t_0)/\tau_f] \quad (4)$$

Under illumination of the green laser, the fitted response and decay time are both 45 ms. Impressively, under illumination of the blue laser, the SnS_2 NFs-based photodetector shows a fast response time ~ 7.3 ms and a decay time ~ 16 ms. Importantly, the response speed of the SnS_2 photodetector under illumination of the blue laser is faster than those of reported SnS_2-based photodetectors [25, 26]. It may be due to two reasons: one is high crystallinity of the SnS_2 NFs, and the other is SnS_2 is more sensitive to incident with shorter wavelength [3].

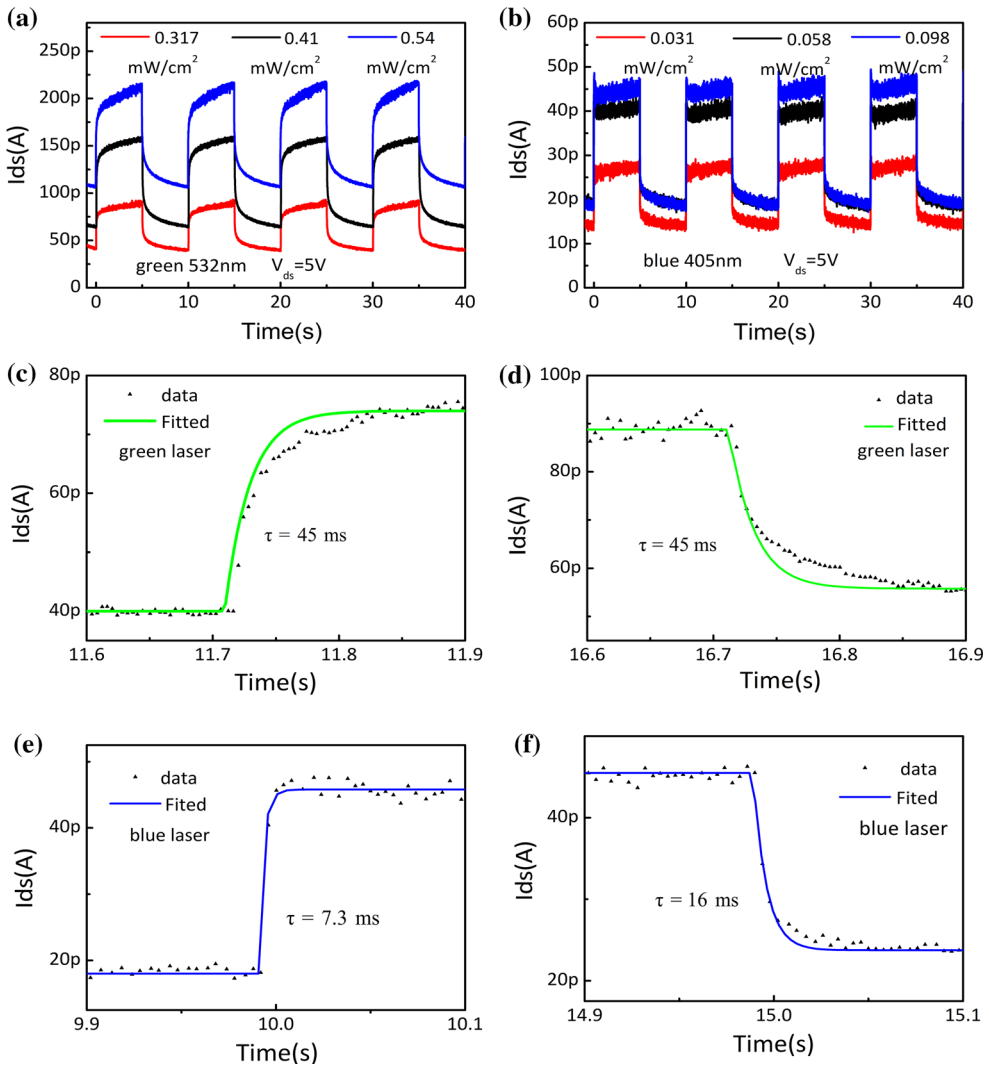

Figure 4 Time-resolved photoresponse of the device at the bias voltage of 5 V, under illumination of the **a** green and **b** blue lasers. **c**, **d** The response time and decay time of the photocurrent under illumination of the green laser at V_{ds} = 5 V. **e**, **f** The response and decay time of the photocurrent under illumination of the blue laser at V_{ds} = 5 V.

Conclusion

In conclusion, we successfully synthesized SnS_2 NFs with high crystallinity and purity via a facile hydrothermal method. The synthesis process was also discussed, and it revealed that the reaction temperature is a more important parameter than the reaction time. Furthermore, through the in-depth study of the photoresponsive of SnS_2 NFs, it is concluded that SnS_2 has reversible and sensitive optical response characteristics. Impressively, the photodetector based on SnS_2 NFs exhibits an excellent performance with a fast response time of 7.3 ms and high detectivity of 1.53×10^{10} Jones. In this work the synthesis process, devices fabrication and responsive characterization of nano-SnS_2 were systematically studied and it may pave the way for the synthesis of LMDs and expand their utilizations for advanced optoelectronics devices.

Acknowledgements

This work was supported by the National Natural Science Foundation of China (Grant No. 61804043), the Natural Science Foundation of Hebei Province, China (Grant No. F2017202058) and the Science and Technology Research Program for Colleges and Universities of Hebei Province, China (Grant No. QN2017041).

Compliance with ethical standards

Conflict of interest The authors declare that they have no conflict of interest.

References

[1] Li H, Li Y, Aljarb A, Shi Y, Li LJ (2018) Epitaxial growth of two-dimensional layered transition-metal dichalcogenides: growth mechanism, controllability, and scalability. Chem Rev 118(13):6134–6150

[2] Fu Y, Cao F, Wu F, Diao Z, Chen J, Shen S, Li L (2018) Phase-modulated band alignment in CdS nanorod_SnS_x nanosheet hierarchical heterojunctions toward efficient water splitting. Adv Funct Mater 28:1706785–1706793

[3] Fan C, Li Y, Lu F, Deng HX, Wei Z, Li J (2016) Wavelength dependent UV–Vis photodetectors from SnS_2 flakes. RSC Adv 6:422–427

[4] Chen H, Chen Y, Zhang H, Zhang DW, Zhou P, Huang J (2018) Suspended SnS_2 layers by light assistance for ultra-sensitive ammonia detection at room temperature. Adv Funct Mater 28:1801035–1801042

[5] Wang P, Hu J, Cao G, Zhang S, Zhang P, Liang C, Wang Z, Shao G (2018) Suppression on allotropic transformation of Sn planar anode with enhanced electrochemical performance. Appl Surf Sci 435:1150–1158

[6] Zhang S, Zhang J, Cao G, Wang Q, Hu J, Zhang P, Shao G (2018) Strong interplay between dopant and SnO_2 in amorphous transparent (Sn, Nb)O_2 anode with high conductivity in electrochemical cycling. J Alloys Compd 735:2401–2409

[7] Wang Q, Fan J, Zhang S et al (2017) In situ coupling of Ti_2O with rutile TiO_2 as a core-shell structure and its photocatalysis performance. RSC Adv 7:54662–54667

[8] Wang L, Fan J, Cao Z, Zheng Y, Yao Z, Shao G, Hu J (2014) Fabrication of predominantly Mn^{4+}-doped TiO_2 nanoparticles under equilibrium conditions and their application as visible-light photocatalyts. Chem Asian J 9:1904–1912

[9] Khot KV, Ghanwat VB, Bagade CS, Mali SS, Bhosale RR, Bagali AS, Dongale TD, Bhosale PN (2016) Synthesis of SnS_2 thin film via non vacuum arrested precipitation technique for solar cell application. Mater Lett 180:23–26

[10] Zheng P, Dai Z, Zhang Y et al (2017) Scalable synthesis of SnS_2/S-doped graphene composites for superior Li/Na-ion batteries. Nanoscale 9:14820–14825

[11] Tao Y, Wu X, Wang W, Wang J (2015) Flexible photodetector from ultraviolet to near infrared based on a SnS_2 nanosheet microsphere film. J Mater Chem C 3:1347–1353

[12] Ou JZ, Ge W, Carey B et al (2015) Physisorption-based charge transfer in two-dimensional SnS_2 for selective and reversible NO_2 gas sensing. ACS Nano 9:10313–10323

[13] Rama G, Jeevanandam P (2018) Synthesis of SnS_2 nanoparticles and their application as photocatalysts for the reduction of Cr(VI). J Nanosci Nanotechnol 18:165–177

[14] Wang L, Zhang X, Gao H, Hu J, Mao J, Liang C, Zhang P, Shao G (2016) 3D CuO network supported TiO_2 nanosheets with applications for energy storage and water splitting. Sci Adv Mater 8:1256–1262

[15] Burton LA, Colombara D, Abellon RD, Grozema FC, Peter LM, Savenije TJ, Dennler G, Walsh A (2013) Synthesis, characterization, and electronic structure of single-srystal SnS, Sn_2S_3, and SnS_2. Chem Mater 25(24):4908–4916

[16] Ahn JH, Lee MJ, Heo H, Sung JH, Kim K, Hwang H, Jo MH (2015) Deterministic two-dimensional polymorphism growth of hexagonal n-type SnS_2 and orthorhombic p-type SnS crystals. Nano Lett 15:3703–3708

[17] Huang Y, Sutter E, Sadowski JT et al (2014) Tin disulfide: an emerging layered metal dichalcogenide semiconductor: materials properties and device characteristics. ACS Nano 8(10):10743–10755

[18] Xia J, Zhu D, Wang L, Huang B, Huang X, Meng XM (2015) Large-scale growth of two-dimensional SnS_2 crystals driven by screw dislocations and application to photodetectors. Adv Funct Mater 25:4255–4261

[19] Zhong M, Wang X, Liu S, Li B, Huang L, Cui Y, Li J, Wei Z (2017) High-performance photodetectors based on Sb_2S_3 nanowires: wavelength dependence and wide temperature range utilization. Nanoscale 9:12364–12371

[20] Mueller T, Xia F, Avouris P (2010) Graphene photodetectors for high-speed optical communications. Nat Photonics 4:297–301

[21] Zhou X, Zhang Q, Gan L, Li H, Zhai T (2016) Large-size growth of ultrathin SnS_2 nanosheets and high performance for phototransistors. Adv Funct Mater 26:4405–4413

[22] Wang H, Zhang L, Chen Z, Hu J, Li S, Wang Z, Liu J, Wang X (2014) Semiconductor heterojunction photocatalysts: design, construction, and photocatalytic performances. Chem Soc Rev 43:5234–5244

[23] Burton LA, Whittles TJ, Hesp D et al (2016) Electronic and optical properties of single crystal SnS_2: an earth-abundant disulfide photocatalyst. J Mater Chem A 4:1312–1318

[24] Yang YB, Dash JK, Xiang Y, Wang Y, Shi J, Dinolfo PH, Lu TM, Wang GC (2016) Tuning the phase and optical properties of ultrathin SnS_x films. J Phys Chem C 120:13199–13214

[25] Huang Y, Deng HX, Xu K et al (2015) Highly sensitive and fast phototransistor based on large size CVD-grown SnS_2 nanosheets. Nanoscale 7:14093–14099

[26] Liu G, Li Z, Chen X et al (2017) Non-planar vertical photodetectors based on free standing two-dimensional SnS_2 nanosheets. Nanoscale 9:9167–9174